ADVANCED MATERIALS INTERFACES
www.advmatinterfaces.de

Underwater Anisotropic 3D Superoleophobic Tracks Applied for the Directional Movement of Oil Droplets and the Microdroplets Reaction

Yang Cheng, Qing Yang, Yao Fang, Jiale Yong, Feng Chen,* and Xun Hou*

In this paper, a simple way to fabricate underwater anisotropic superoleophobic tracks is reported for manipulating underwater oil droplets by the femtosecond laser etching and the oxygen plasma treatment. Laser ablation is able to generate micro/nanoscale hierarchical structures on the poly(dimethylsiloxane) (PDMS) surface. The textured PDMS surface is further turned from superhydrophobicity to hydrophilicity and underwater superoleophobicity by subsequent oxygen plasma irradiation. Underwater anisotropic 3D superoleophobic tracks can also be fabricated on the PDMS surface by the laser etching method. The width of the tracks depends on the laser-treated area, while the depth of the tracks increases with increasing the laser power and the scanning number and with decreasing the laser scanning speed/space. The underwater superoleophobic 3D tracks show ultralow adhesion and anisotropic sliding property to oil droplets, thereby allow the underwater oil droplets to move just along the track. A microdroplets reaction is proposed based on the underwater superoleophobic tracks. There is no loss of the reactants during the whole reaction process. The anisotropic sliding property of underwater organic droplets will potentially have enormous applications in droplet manipulation, microfluidics system, surface lab-chip devices, and chemical engineering.

1. Introduction

Anisotropic wettability attracts broad interests because of its wide applications, such as drag reduction,[1–3] anti-bioadhesion,[4–6] small droplet manipulation,[7–12] chemical shielding,[13,14] and microfluidics.[15–18] In nature, rice leaf has three-level geometrical structures with anisotropic superhydrophobicity.[19,20] On the rice leaf surface, microscale papillae and nanostructures directionally arrange on the surface of the sub-millimeter-scale grooves.[21] The superhydrophobicity is attributed to the micro/nanoscale hierarchical rough structures and low surface energy. The macrogrooves endow the rice leaf with the anisotropic sliding property for water droplets, so the dewdrops more easily roll to the root of rice leaf and help rice to well survive in an arid environment. The ridging nanostripes and flexible nanotips directionally cover on the butterfly wing, which exhibits superhydrophobicity and unidirectional water adhesion.[14] This unique structure allows rain droplets to easily roll along the radial-outward direction on the butterfly wing, reducing the flight resistance in a rainy day.[22] The filefish skin shows superoleophobicity and unidirectional oil adhesion in water. Many hook-like spines distribute on the filefish skin. Due to the directional arrangement of the spines, underwater oil droplets can easily roll off the filefish skin along the head-to-tail direction but tend to be pinned in the opposite direction, enabling the fish to swim in the oil-polluted water.[23,24]

Inspired by natural surfaces, Yong et al. constructed directional patterns on poly(dimethylsiloxane) (PDMS) surface by femtosecond laser ablation. The prepared surface showed anisotropic superhydrophobicity.[25] Wu et al. prepared the three-level (macro/micro/nanoscale) anisotropic microstructures by the combination of photolithography and imprint lithography.[20] Water droplets on the sample surface were more inclined to roll along the macroscale grooves. Brueck and co-worker used multibeam-laser interference lithography to fabricate a 1D nano-patterned surface and observed the anisotropic wetting behavior on such a surface.[26] Until now, a large number of anisotropic superhydrophobic surfaces have been fabricated, and these surfaces are successfully applied to manipulate water droplets, e.g., the directional movement of water droplets.[27–31] However, the directional and no-loss movement of oil droplets in a water medium has still rarely been reported. The lossless manipulation of oil droplets is of great importance in various miniature systems for both chemical and biological applications, such as high-throughput

Dr. Y. Cheng, Prof. Q. Yang
School of Mechanical Engineering
Xi'an Jiaotong University
Xi'an 710049, P. R. China
Dr. Y. Cheng, Prof. Q. Yang, Dr. Y. Fang, Dr. J. Yong, Prof. F. Chen
The International Joint Research Laboratory for Micro/Nano Manufacturing and Measurement Technologies
Xi'an Jiaotong University
Xi'an 710049, P. R. China
E-mail: jlyong@xjtu.edu.cn; chenfeng@mail.xjtu.edu.cn
Dr. Y. Fang, Dr. J. Yong, Prof. F. Chen, Prof. X. Hou
State Key Laboratory for Manufacturing System Engineering and Shaanxi Key Laboratory of Photonics Technology for Information
School of Electronics and Information Engineering
Xi'an Jiaotong University
Xi'an 710049, P. R. China
The ORCID identification number(s) for the author(s) of this article can be found under https://doi.org/10.1002/admi.201900067.

DOI: 10.1002/admi.201900067

detection and analysis. In microchemical reaction, the lossless manipulation of oil droplets reduces the volatilization of reactants and maximally captures the valuable reactants, which is used to analyze.[4,18,24,32]

Here, we report a facile strategy to prepare underwater anisotropic 3D superoleophobic tracks on the PDMS surface by the femtosecond laser etching and the oxygen plasma treatment.[1,33] Laser ablation can create a hierarchical rough microstructure on the PDMS surface.[34] Further oxygen plasma treatment is able to graft hydrophilic groups on the rough PDMS and then endows the PDMS surface with hydrophilicity and underwater superoleophobicity.[35] Track structure is also designed on the PDMS surface and shows underwater anisotropic oil wettability. The influence of the laser power, laser scanning speed/space, and scanning number (SN) on the etching depth of the track is carefully investigated. It is found that the underwater oil droplets prefer to move along the 3D superoleophobic tracks. A microchemical reaction is also achieved by using the underwater 3D superoleophobic tracks.

2. Results and Discussion

2.1. Surface Morphology

The surface morphology of the femtosecond laser-ablated PDMS is influenced by the laser scanning speed and the scanning space during femtosecond laser treatment.[36] The manner of femtosecond laser processing is depicted in **Figure 1**a. The PDMS sheet was mounted on a motorized 3D computer-controlled translation stage. The femtosecond laser beam was focused onto the PDMS surface by an objective lens. Average

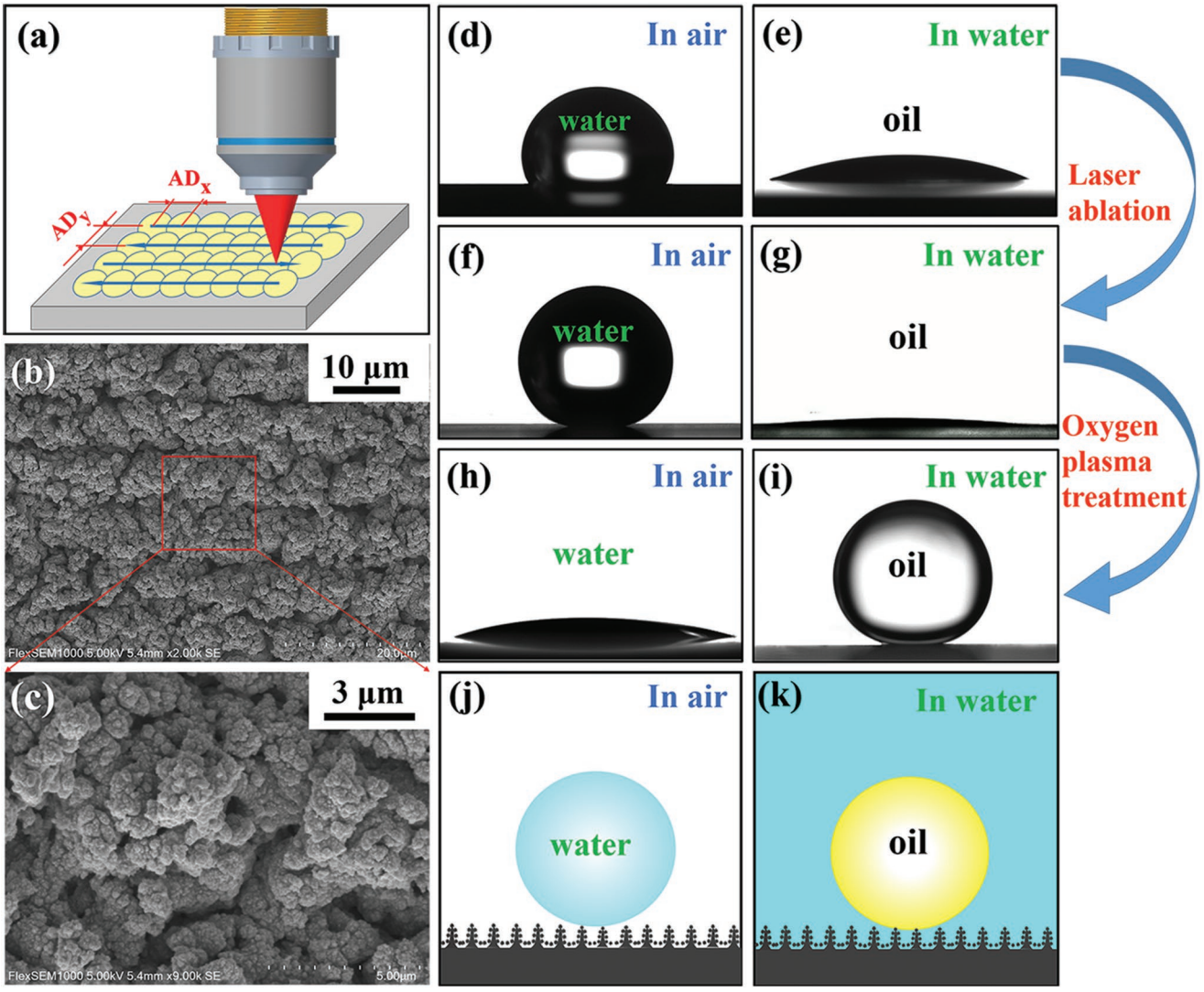

Figure 1. Surface morphology and wettability of the laser-treated PDMS surface. a) Schematic illustration of the laser processing. b,c) SEM images of the PDMS surface after laser ablation. d) Water droplet on the flat PDMS surface in air. e) Oil droplet on the flat PDMS surface in water. f) Water droplet on the laser-ablated PDMS surface in air. g) Oil droplet on the laser-ablated PDMS surface in water. h) Water droplet on the plasma-irradiated rough PDMS surface in air. i) Oil droplet on the plasma-irradiated rough PDMS surface in water. j) Cassie wetting state between a water droplet and the laser-induced rough PDMS surface. k) Underwater Cassie wetting state between an oil droplet and the plasma-irradiated rough PDMS surface.

distance, AD, is the mean distance of the adjacent laser ablation points, which depends on the laser scanning speed and the scanning space. AD_x and AD_y are the distance of the adjacent laser points in the crosswise direction and in the lengthways direction, respectively. AD_x is determined by the laser scanning speed and equals the scanning speed divided by the pulse repetition rate, while AD_y is determined by the space of the adjacent laser scanning lines. In our experiment, we make $AD = AD_x = AD_y$. Hence, AD increases with the increase of the scanning speed and the scanning space. Figure 1b,c shows the scanning electron microscopy (SEM) images of the PDMS surface after femtosecond laser ablation. The surface was ablated by the laser at the power of 40 mW and the AD of 8 µm. Abundant loose and porous coral-like protrusions with the size of tens of micrometer distribute on the PDMS surface (Figure 1b). The surfaces of the coral-like protrusions are further covered with hundreds of accumulated or sporadic nanoparticles (Figure 1c). Such micro/nanoscale hierarchical structures result from the laser ablation and the resolidification of the ejected particles.

2.2. Surface Wettability

PDMS is an intrinsically hydrophobic and underwater oleophilic substrate. Water droplet on the flat PDMS has a water contact angle (WCA) of 110° in air (Figure 1d), and underwater oil droplet on the flat PDMS surface has an oil contact angle (OCA) of 22° (Figure 1e). After the formation of surface microstructure by the femtosecond laser treatment, the rough PDMS surface shows superhydrophobicity with a WCA of 160° and a sliding angle (SA) of 1° (Figure 1f). Such ultralow adhesive superhydrophobicity is ascribed to the Cassie wetting state of the water droplet on the rough PDMS surface (Figure 1j). The contact area between the water droplet and the treated PDMS surface is remarkably reduced by the laser-induced hierarchical rough microstructure. Regarding the oil droplet, it can quickly spread out on the rough PDMS surface in water. The measured OCA is only 6° (Figure 1g), so the original laser-ablated PDMS surface exhibits underwater superoleophilicity. Oxygen plasma treatment is a common way to introduce hydrophilic groups onto the PDMS surface. The original methyl ($-CH_3$) of the PDMS surface is converted into the hydrophilic group of hydroxyl (−OH) under oxygen plasma irradiation.[16,37] Hence, the laser-induced rough PDMS surface turns from superhydrophobicity to hydrophilicity after further being irradiated by oxygen plasma. The WCA of a water droplet on the resultant surface decreases to 16° (Figure 1h). By contrast, the underwater oil droplet can keep a spherical shape with an OCA of 161° on the plasma-irradiated rough PDMS surface (Figure 1i). The oil droplet will easily roll off when the PDMS surface is slightly tilted at 1°. Therefore, the laser-ablated PDMS surface shows underwater superoleophobicity and ultralow oil adhesion after oxygen plasma treatment. The oil droplet on such a surface is at the underwater Cassie state, as shown in Figure 1k. Water fully wets the rough microstructure of the PDMS surface because of the hydrophilicity, forming a trapped water cushion between the oil droplet and the rough surface microstructure. The water cushion greatly reduces the contact area between the oil droplet and the PDMS surface, resulting in the underwater superoleophobicity and extremely low oil-adhesion of the plasma-treated rough PDMS surface.

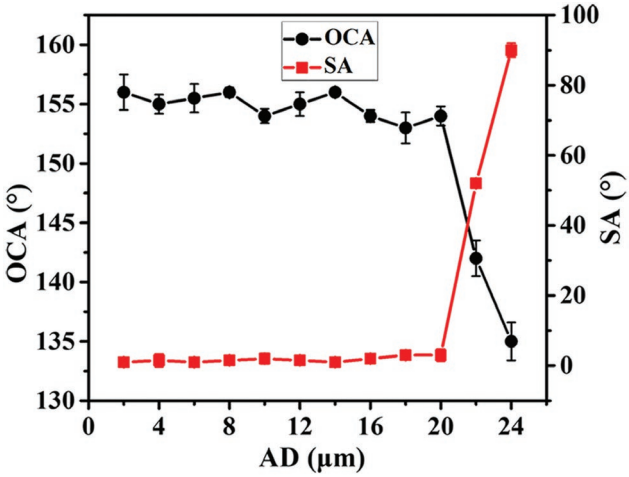

Figure 2. Relationship between the underwater oil wettability and the AD.

The surface wettability of the femtosecond laser-ablated PDMS is influenced by the AD. **Figure 2** depicts the underwater oil wettability of the as-prepared surface fabricated at different AD values (laser power of 40 mW). The measured OCA values are larger than 150° and the SA values are smaller than 10° when AD is smaller than 20 µm, so the as-prepared surfaces exhibit excellent underwater superoleophobicity and ultralow oil adhesion. With AD increasing from 20 to 24 µm, the OCA decreases from 154° to 135°, while the SA sharply increases from 3° to 90° (oil droplet sticks on the surface even when the sample is vertical). The result reveals that the wettability of the as-prepared surfaces changes from underwater superoleophobicity to ordinary oleophobicity with high oil adhesion, because the surface roughness of the laser-ablated PDMS reduces with increasing AD. Therefore, underwater superoleophobicity can be obtained on the PDMS surface with AD no larger than 20 µm.

2.3. Underwater 3D Superoleophobic Track

Laser ablation is also an etching process. The etching depth is mainly affected by the laser power, AD, and SN. As shown in **Figure 3**a, the etching depth increases with increasing the laser power (AD = 8 µm, SN = 1). A higher laser power generally results in the stronger ablation process and materials removal, generating a deeper groove. Figure 3b shows the influence of the AD on the etching depth (laser power = 40 mW, SN = 1). With the increase of AD, the etching depth decreases obviously. A larger AD value means that the scanning speed/space is higher in the laser processing, so the number of the laser pulses that acting on per area is smaller. Fewer laser pulses lead to a weaker ablation as well as a smaller etching depth. Multiple laser treatments are also a simple way to increase the depth of the laser-etched domain. It is found that the etching depth linearly increases with increasing SN (Figure 3c–e).

Underwater 3D superoleophobic tracks can be easily prepared on the PDMS surface by two steps of laser etching and oxygen plasma treatment. Multiple laser etching increases the

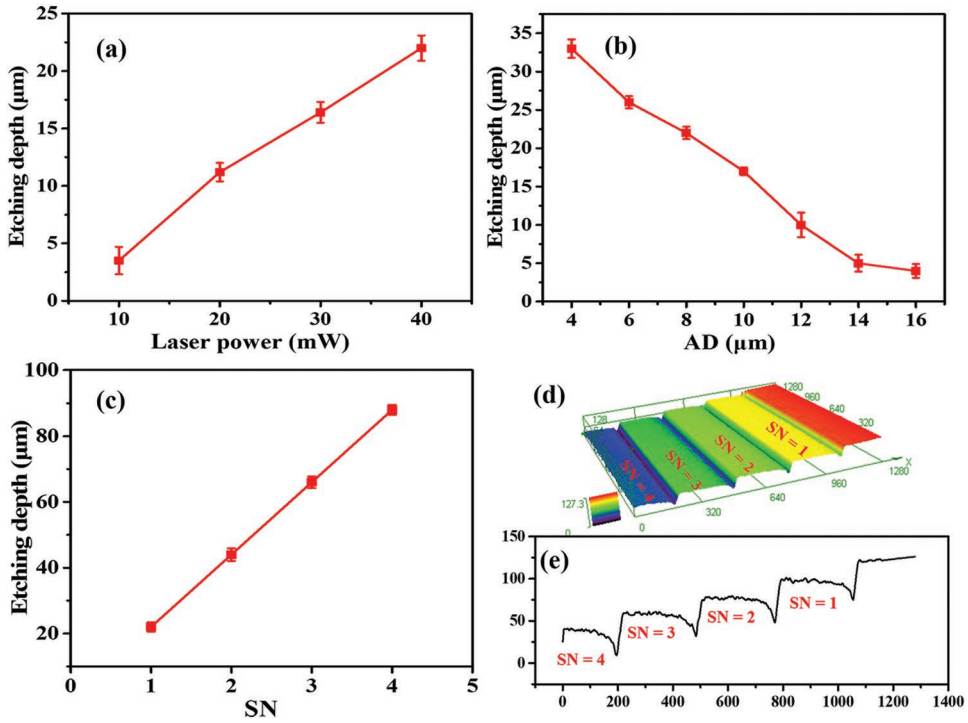

Figure 3. Influence of the a) laser power, b) AD, and c) SN on the etching depth. d) 3D profile and e) cross-sectional profile of the sample surface that is ablated by laser for different times.

etching depth and generates microstructures.[35] The oxygen plasma treatment grafts hydrophilic groups on the tracks. Microstructures and hydrophilic groups commonly endow the tracks with underwater superoleophobicity. **Figure 4**a depicts the surface topography of a laser-etched track array. The track domain is etched by femtosecond laser for four times at the laser power of 40 mW and the AD of 8 μm. The width (W) of the tracks is measured to be 200 μm, and the height (H) of the tracks is 88 μm. Both the bottom and top surfaces of the tracks are covered with rough surface microstructures. The bottom of the track shows the laser-induced hierarchical coral-like protrusions (Figure 4b). Surprisingly, there are still many micro-nanoparticles distributing on the top surface of the tracks, although such an area is not ablated by laser (Figure 4c). Such micro-nanoparticles mainly come from the ejected particles in the etching process. The as-prepared 3D tracks are uniform in shape (Figure 4d,e). Because of the existence of the laser-induced surface microstructures, the tracks present excellent underwater superoleophobicity after oxygen plasma treatment. The height of the underwater 3D superoleophobic tracks can be designed through adjusting the laser power, AD, and SN, while the width of 3D tracks depends on the laser-etched area.[29,38]

2.4. Anisotropic Sliding Property on the Track

The sliding behavior of an underwater oil droplet on the as-prepared 3D superoleophobic tracks was carefully investigated, including the SAs along the track direction ($SA_{//}$) and the perpendicular direction ($SA_{\perp}$), respectively. **Figure 5**a shows the influence of the H on the SA at $W \equiv 1000$ μm. It can be found that the $SA_{//}$ is always less than 2° and is almost not affected by the H. By contrast, the $SA_{\perp}$ increases from 3° to 6° as the H increases from 22 to 88 μm. When the H is smaller than 88 μm, the oil droplet touches the bottom of the track but is not sandwiched by two side walls of the track (Figure 5c). With the increase of the H, the height of the side wall increases, so the potential energy that allows the oil droplet to derail also increases. Therefore, the $SA_{\perp}$ increases with H. When the H increases to 88 μm, the oil droplet in the track can be just in contact with the bottom and both side walls of the track (Figure 5d). At present, the different value of SA ($\Delta SA = SA_{\perp} - SA_{//}$) is 5° and the anisotropic sliding property is the most obvious. If the H is further increases to 110 μm, the oil droplet will leave the bottom of the track and be lifted up by the end edges of two side walls (Figure 5e). The adhesion between the oil droplet and the bottom of the track disappears, so the $SA_{\perp}$ slightly decreases to 5° at $H = 110$ μm. As shown in Figure 5a, the greatest sliding anisotropy is 5° for the underwater oil droplet on the 3D track with H of 88 μm and W of 1000 μm.

W is another crucial parameter of the track, which affects the anisotropic sliding property for the underwater oil droplets. Figure 5b shows the relationship between the anisotropic sliding property ($SA_{//}$, $SA_{\perp}$, and ΔSA) and the W ($H \equiv 88$ μm). The $SA_{//}$ is almost unaffected by the W because it is less than 2° with the W ranging from 600 to 1400 μm. Regarding the $SA_{\perp}$, it increases from 4° to 6° as the W increases from 600 to 1000 μm. When the W is smaller than 1000 μm, the oil droplet is lifted up by two side walls of the track and does not contact with the bottom of the track (Figure 5f). As the W increases from 600 to 1000 μm, the depth of the oil droplet embedding in the track increases. The potential energy that allows

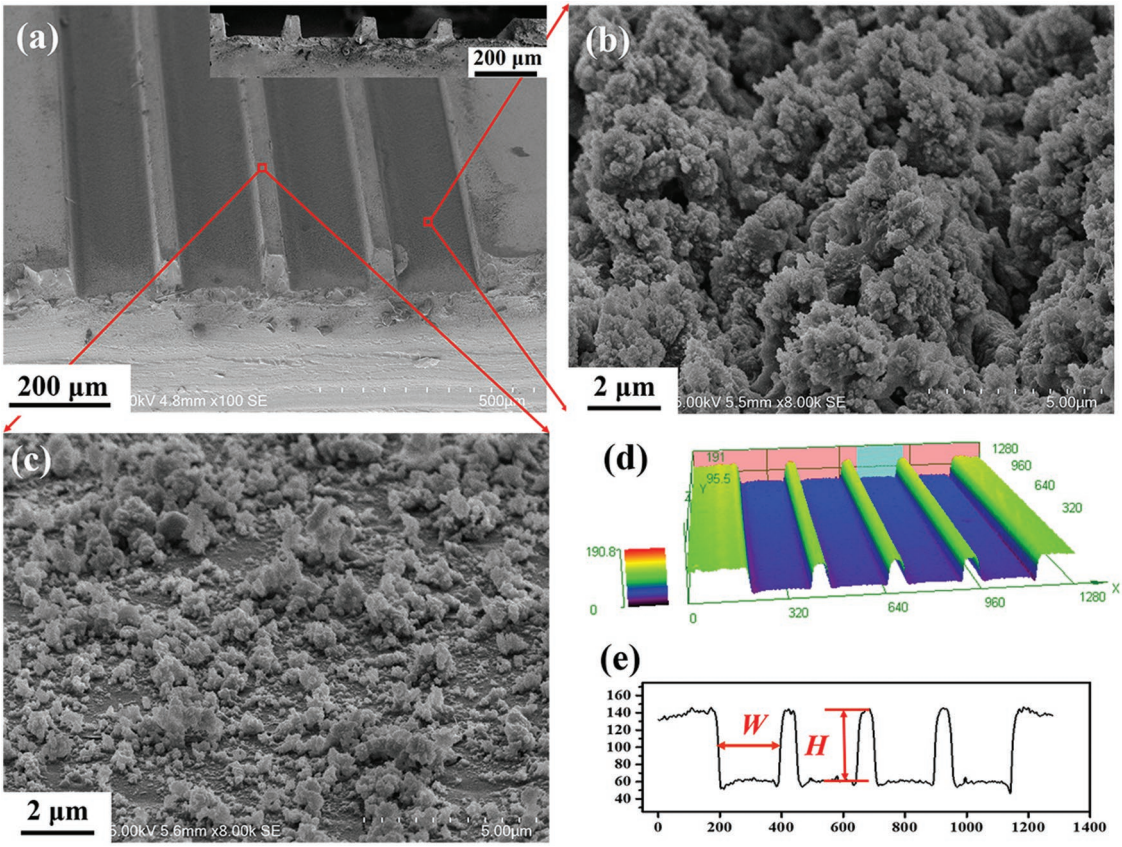

Figure 4. Morphology of the laser-etched track structure. a) 45°-tilted view of the SEM image of the tracks. The inset is the cross-sectional SEM image. The magnified SEM images of b) the bottom surface and c) the top surface of the tracks. d) 3D profile and e) cross-sectional profile of the track array.

the oil droplet to derail also increases, so the $SA_{\perp}$ increases with W. When the W increases to 1000 µm, the oil droplet exactly touches the bottom and both two side walls of the track (Figure 5g). In this case, the depth of the oil droplet embedding in the track reaches the maximum. When the W is larger than 1000 µm, the oil droplet can be in contact with the bottom and just one side wall of the track (Figure 5h). As the W continually increases from 1000 to 1400 µm, the depth of the oil droplet embedding in the track does not change, so the $SA_{\perp}$ keeps constant. As shown in Figure 5b, the optimal anisotropic sliding property ($\Delta SA = 5°$) for the oil droplet is obtained on the 3D track with W of 1000 µm and H of 88 µm.

From Figure 5a,b, it can be found that the $SA_{\perp}$ is always larger than the $SA_{//}$ for an oil droplet on the underwater 3D superoleophobic tracks in the water medium. The results indicate that the tracks show anisotropic sliding property to oil droplets, allowing the underwater oil droplets to only move along the 3D tracks.

2.5. Microdroplets Reaction Device

The underwater 3D superoleophobic tracks can be applied in the dynamic transportation of underwater oil droplets.[8] A device that can achieve microdroplets reaction based on the underwater superoleophobic tracks was designed. As an example, 6 µL bromine in carbon tetrachloride solution (concentration = 30%, v/v) and 6 µL styrene in carbon tetrachloride solution (concentration = 30%, v/v) were adopted as two reactants. As shown in **Figure 6**a and Movie S1 (Supporting Information), the styrene droplet was first placed on the track. Then, the bromine droplet was also dispensed onto the track. Driven by gravity, the bromine droplet directionally moved along the track from high to low when the track was slightly tilted. The styrene droplet and the bromine droplet coalesced together after contacting with each other. The saturated C=C in styrene was broken. As the bromine atom added in an unsaturated C—C, colorless 1,2-dibromoethylbenzene generated. We can see that the orange-brown bromine droplet gradually faded in the reaction. Meanwhile, an addition reaction occured without the volume loss in the whole reaction process. The corresponding schematic diagram is shown in Figure 6b. According to the order of the microdroplets reaction, the track structure can be designed, thereby reactants can be dispensed in order and the sequence of chemical reaction can be controlled. The result reveals that the underwater anisotropic superoleophobic track is successfully used in the microdroplets reaction for a small amount of reactants.

3. Conclusions

Anisotropic sliding track structure with underwater superoleophobicity is prepared on the PDMS surface by the femtosecond

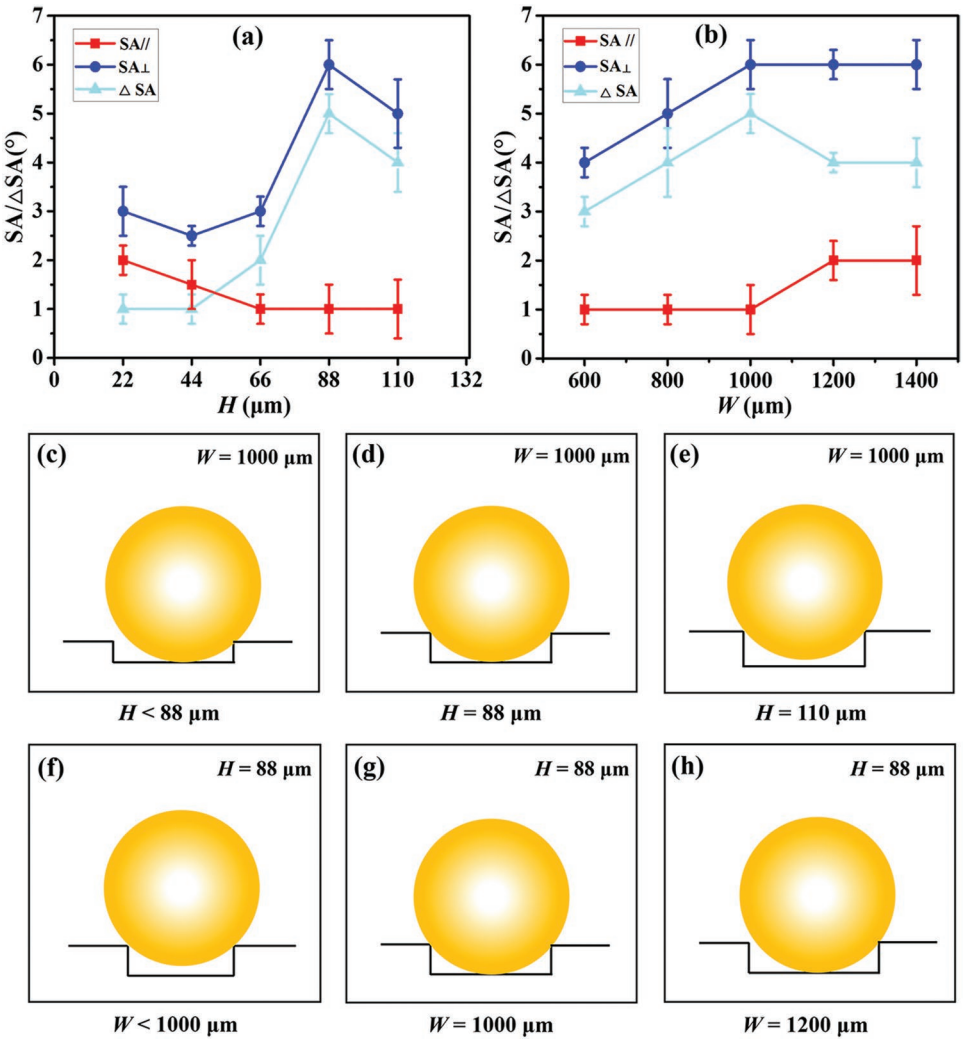

Figure 5. Anisotropic sliding property for the underwater oil droplets on the tracks. Relationship between the SA and a) *H* and b) *W*. The schematic illustration of the contact state between the oil droplet and the resultant tracks: c) $H < 88$ μm, d) $H = 88$ μm, and e) $H = 110$ μm (in the condition of $W = 1000$ μm). The schematic illustration of the contact state between the oil droplet and the resultant tracks: f) $W < 1000$ μm, g) $W = 1000$ μm, and h) $W = 1200$ μm (in the condition of $H = 88$ μm).

laser etching and the oxygen plasma treatment. The laser ablation generates hierarchical rough microstructure on the PDMS surface. Subsequent oxygen plasma treatment can graft hydrophilic groups onto the rough PDMS surface and change the rough PDMS from superhydrophobicity to hydrophilicity and underwater superoleophobicity. The underwater oil droplet on the resultant PDMS surface has an OCA of 161° and can easily roll off when the PDMS surface is slightly tilted at 1°. 3D tracks with underwater superoleophobic surfaces can also be fabricated on the PDMS substrate by laser etching manner. The width of the tracks depends on the laser-treated area, while the height of the tracks increases with increasing the laser power and the scanning number, and decreasing the laser scanning speed/space. The underwater 3D superoleophobic track shows ultralow oil adhesion and anisotropic sliding property, with an $SA_{//}$ of 1° and an $SA_{\perp}$ of 6° to underwater oil droplets; i.e., the underwater anisotropic 3D superoleophobic tracks prefer to allow the oil droplets to move along the tracks in water. An addition reaction between the styrene and bromine microdroplets is realized on the underwater superoleophobic track, without the loss of reactants during the whole reaction process. Such underwater anisotropic 3D superoleophobic tracks will have significant applications in the oil droplet manipulation, oil droplet capture, chemical shielding, and microfluidics.

4. Experimental Section

The PDMS thin films were prepared from a 10:1 mixture (by volume) of the prepolymer (DC-184, Dow Corning) and the curing agent, curing at 100 °C for 1.5 h.

A regenerative amplified Ti: sapphire laser system (Coherent Libra-usp-he) that produces femtosecond laser pulses (pulse width = 50 fs; central wavelength = 800 nm; repetition rate = 1 kHz) was used to ablate the PDMS surface. The PDMS sheet was mounted on a motorized 3D computer-controlled translation stage. The laser beam was focused onto the PDMS surface by an objective lens (10×, NA = 0.3, Nikon).

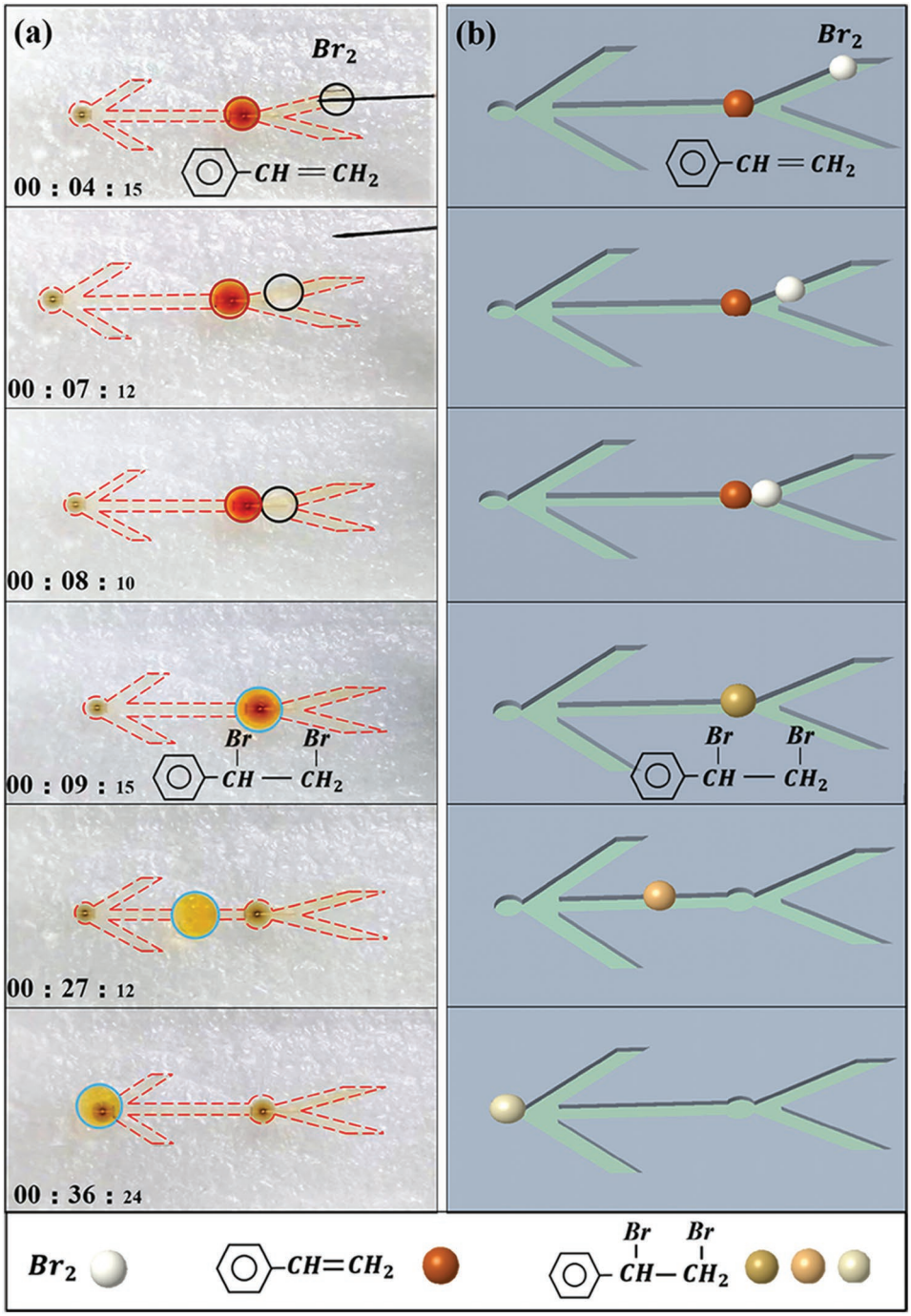

Figure 6. a) The process of microdroplets reaction between the bromine in carbon tetrachloride solution and the styrene in carbon tetrachloride solution on the 3D superoleophobic track in water. The dotted line is the contour of the track and the solid line is the contour of the droplets. b) Schematic diagram of the process of the microdroplets reaction.

The manner of femtosecond laser processing is shown in Figure 1a. The femtosecond laser-ablated PDMS surface was irradiated by oxygen plasma in a PR-3 plasma reactor (Heshi Technology, China) for 30 s (50 W).

The morphology of the laser-ablated PDMS surfaces was observed by a Flex1000 scanning electron microscope (Hitachi, Japan). The 3D profile of the sample surface was measured via a LEXT-OLS4000 laser confocal microscopy (Olympus, Japan). The CA and the SA of 6 µL water droplets and 6 µL oil (chloroform) droplets on the sample surfaces were measured by a JC2000D contact angle system (Powereach, China), respectively. The process of manipulating droplets was recorded by a charge-coupled device camera system.

Supporting Information

Supporting Information is available from the Wiley Online Library or from the author.

Acknowledgements

This work was supported by the National Natural Science Foundation of China under Grant Nos. 61875158, U1630111, 61435005, and 61805192, the National Key Research and Development Program of China under Grant No. 2017YFB1104700, the China Postdoctoral Science Foundation under Grant No. 2016M600786, the Collaborative Innovation Center of Suzhou Nano Science and Technology, and the Instrument Analysis Center of Xi'an Jiaotong University.

Conflict of Interest

The authors declare no conflict of interest.

Keywords

anisotropic wettability, directional movement, femtosecond laser, microdroplets reaction, underwater superoleophobicity

Received: January 10, 2019
Revised: February 17, 2019
Published online: April 8, 2019

[1] J. Yong, F. Chen, Q. Yang, D. Zhang, U. Farooq, G. Du, X. Hou, *J. Mater. Chem. A* **2014**, *2*, 8790.
[2] X. Hao, W. Cui, L. Li, H. Li, A. M. Khan, N. He, *J. Mater. Process. Technol.* **2018**, *260*, 1.
[3] Y. Liu, H. Gu, Y. Jia, J. Liu, H. Zhang, R. Wang, B. Zhang, H. Zhang, Q. Zhang, *Chem. Eng. J.* **2019**, *356*, 318.
[4] J. Yong, F. Chen, Q. Yang, J. Huo, X. Hou, *Chem. Soc. Rev.* **2017**, *46*, 4168.
[5] W. Liu, X. Liu, J. Fangteng, S. Wang, L. Fang, H. Shen, S. Xiang, H. Sun, B. Yang, *Nanoscale* **2014**, *6*, 13845.
[6] V. Jokinen, E. Kankuri, S. Hoshian, S. Franssila, R. H. A. Ras, *Adv. Mater.* **2018**, *30*, 1705104.
[7] G. Li, Y. Lu, P. Wu, Z. Zhang, J. Li, W. Zhu, Y. Hu, D. Wu, J. Chu, *J. Mater. Chem. A* **2015**, *3*, 18675.
[8] B. Su, S. Wang, Y. Song, L. Jiang, *Soft Matter* **2011**, *7*, 5144.
[9] S. Huang, J. Song, Y. Lu, F. Chen, H. Zheng, X. Yang, X. Liu, J. Sun, C. J. Carmalt, I. P. Parkin, W. Xu, *ACS Appl. Mater. Interfaces* **2016**, *8*, 2942.
[10] J. Huo, Q. Yang, F. Chen, J. Yong, Y. Fang, J. Zhang, L. Liu, X. Hou, *Langmuir* **2017**, *33*, 3659.
[11] Y. Zhao, J. Fang, H. Wang, X. Wang, T. Lin, *Adv. Mater.* **2010**, *22*, 707.
[12] P. Wang, W. Wang, T. Ci, L. Li, H. Han, *Appl. Surf. Sci.* **2018**, *455*, 980.
[13] S. Pan, A. K. Kota, J. M. Mabry, A. Tuteja, *J. Am. Chem. Soc.* **2013**, *135*, 578.
[14] Y. Zheng, X. Gao, L. Jiang, *Soft Matter* **2007**, *3*, 178.
[15] B. Xu, Y. Zhang, H. Xia, W. Dong, H. Ding, H. Sun, *Lab Chip* **2013**, *13*, 1677.
[16] D. Wu, S. Wu, Q. Chen, S. Zhao, H. Zhang, J. Jiao, J. A. Piersol, J. Wang, H. Sun, L. Jiang, *Lab Chip* **2011**, *11*, 3873.
[17] J. Songok, M. Tuominen, H. Teisala, J. Haapanen, J. Mäkelä, J. Kuusipalo, M. Toivakka, *ACS Appl. Mater. Interfaces* **2014**, *6*, 20060.
[18] J. Yong, F. Chen, Q. Yang, Z. Jiang, X. Hou, *Adv. Mater. Interfaces* **2018**, *5*, 1701370.
[19] L. Feng, S. Li, Y. Li, H. Li, L. Zhang, J. Zhai, Y. Song, B. Liu, L. Jiang, D. Zhu, *Adv. Mater.* **2002**, *14*, 1857.
[20] D. Wu, J. Wang, S. Wu, Q. Chen, S. Zhao, H. Zhang, H. Sun, L. Jiang, *Adv. Funct. Mater.* **2011**, *21*, 2927.
[21] S. Nishimoto, B. Bhushan, *RSC Adv.* **2013**, *3*, 671.
[22] Z. Guo, W. Liu, B. Su, *J. Colloid Interface Sci.* **2011**, *353*, 335.
[23] Y. Cai, L. Lin, Z. Xue, M. Liu, S. Wang, L. Jiang, *Adv. Funct. Mater.* **2014**, *24*, 809.
[24] T. Jiang, Z. Guo, W. Liu, *J. Mater. Chem. A* **2015**, *3*, 1811.
[25] J. Yong, Q. Yang, F. Chen, D. Zhang, G. Du, H. Bian, J. Si, X. Hou, *RSC Adv.* **2014**, *4*, 8138.
[26] D. Xia, S. R. J. Brueck, *Nano Lett.* **2008**, *8*, 2819.
[27] Y. Zhang, H. Xia, E. Kim, H. Sun, *Soft Matter* **2012**, *8*, 11217.
[28] H. Mertaniemi, V. Jokinen, L. Sainiemi, S. Franssila, A. Marmur, O. Ikkala, R. H. Ras, *Adv. Mater.* **2011**, *23*, 2911.
[29] Y. Fang, J. Yong, F. Chen, J. Huo, Q. Yang, J. Zhang, X. Hou, *Adv. Mater. Interfaces* **2018**, *5*, 1701245.
[30] D. Wu, S. Wu, Q. Chen, Y. Zhang, J. Yao, X. Yao, L. Niu, J. Wang, L. Jiang, H. Sun, *Adv. Mater.* **2011**, *23*, 545.
[31] J. Long, P. Fan, D. Jiang, J. Han, Y. Lin, M. Cai, H. Zhang, M. Zhong, *Adv. Mater. Interfaces* **2016**, *3*, 1600641.
[32] Z. Xu, L. Wang, C. Yu, K. Li, Y. Tian, L. Jiang, *Adv. Funct. Mater.* **2018**, *28*, 1703970.
[33] J. Yong, F. Chen, M. Li, Q. Yang, Y. Fang, J. Huo, X. Hou, *J. Mater. Chem. A* **2017**, *5*, 25249.
[34] J. Yong, S. C. Singh, Z. Zhan, F. Chen, C. Guo, *ACS Appl. Mater. Interfaces* **2019**, *11*, 8667.
[35] S. H. Tan, N. Nguyen, Y. C. Chua, T. G. Kang, *Biomicrofluidics* **2010**, *4*, 032204.
[36] J. Yong, S. C. Singh, Z. Zhan, F. Chen, C. Guo, *Langmuir* **2019**, *35*, 921.
[37] J. Yong, F. Chen, J. Huo, Y. Fang, Q. Yang, J. Zhang, X. Hou, *Nanoscale* **2018**, *10*, 3688.
[38] J. Yong, Q. Yang, F. Chen, D. Zhang, G. Du, H. Bian, J. Si, F. Yun, X. Hou, *Appl. Surf. Sci.* **2014**, *288*, 579.

